THE ASTROPHYSICAL JOURNAL, 423:326–333, 1994 March 1

SPECTRAL IMAGING OF THE ORION BAR AT 3.3, 8.4, AND 11.3 MICRONS: COMPARISON WITH A FLUORESCENT POLYCYCLIC AROMATIC HYDROCARBON MODEL

JESSE BREGMAN,[1] KRISTEN LARSON,[2] DAVID RANK,[2] AND PASQUALE TEMI[2]

Received 1993 February 25; accepted 1993 September 13

ABSTRACT

Spectral images were obtained of the Orion Bar which sample polycyclic aromatic hydrocarbon (PAH) emission at 3.3, 8.4, and 11.3 μm. The images are strikingly different even though they all sample PAH emission. In particular, the 3.3 and 11.3 μm images sample PAH emission from C-H bonds, yet the 3.3 μm image contains many small bright knots while the 11.3 μm image is much more uniform. For comparison with a fluorescent PAH model, a data set was created from the measured intensities of 250 locations in each image. From the comparison, we conclude that: (1) the size distribution of PAHs varies within the Bar, with the bright 3.3 μm knots containing the largest proportion of small PAHs; (2) the points along the front of the Bar have emission cross sections characteristic of neutral PAHs while within the Bar, the emission cross sections are different, consistent with the PAHs being charged; (3) the PAHs along the front of the Bar are larger than average for the Bar; (4) emission along the back of the Bar is consistent with PAH emission in an attenuated UV radiation field; (5) there is no evidence for PAH dehydrogenation.

Subject headings: dust, extinction — infrared: ISM: continuum — ISM: individual (Orion Nebula) — ISM: molecules

1. INTRODUCTION

The infrared spectra of many planetary nebulae, H II regions, galactic nuclei, reflection nebulae, and WC stars are dominated by a set of narrow emission features and broad plateaus which for many years were called the "unidentified infrared bands." These bands have been attributed to several carbon-rich species, including polycyclic aromatic hydrocarbon (PAH) molecules and PAH clusters (Leger & Puget 1984; Allamandola, Tielens, & Barker 1985), hydrogenated amorphous carbon (HAC) particles (Duley & Williams 1981), and quenched carbonaceous composite (QCC) particles (Sakata et al. 1984). All of these suggested materials contain only carbon and hydrogen atoms, and are usually dominated by aromatic (sp^2) carbon skeletons (Robertson & O'Reilly 1987). If the narrow bands are from PAH molecules, then PAHs contain 1%–10% of the interstellar carbon, making them the most abundant molecular species in the interstellar medium after H_2 and CO.

There are several pieces of evidence that support the identification of PAHs as the source of the emission bands. Cohen et al. (1986) showed that the emission feature strength in planetary nebulae correlated with the C/O ratio, indicating that the emission features originated in a carbon-based compound. Examination of laboratory spectra of PAHs had indicated that if the narrow emission bands were from PAHs, then there should be additional weak bands at 5.2 μm and between 11.3 and 13 μm. Subsequent observations detected these bands (Allamandola et al. 1989; Roche, Aitken, & Smith 1989; Witteborn et al. 1989). Recently, Bregman et al. (1993) have shown that in HD 44179, the absorption cross section for the 11.3 μm band is significantly greater than for the 3.3 μm band, in agreement with laboratory measurements of PAHs. Thus, there is strong evidence that at least the narrow emission bands are due to PAH molecules.

In PAH molecules, the 3.3 μm band is due to a C-H stretch, the 8.6 and 11.3 μm bands are due to C-H bends (in and out of plane, respectively), and the 6.2 and 7.7 μm bands are C-C modes. Allamandola et al. (1985) had also suggested that the bands observed just longward of the 3.3 μm band, the strongest occurring at 3.4 μm, were due to excited states of PAH molecules. Following up on this suggestion, Bregman (1989) compared existing data for band ratios for the 3.3, 3.4, and 11.3 μm bands with the ratios expected if all of these bands were due to C-H modes in PAHs. This comparison showed that the data did not fit the theory if the same size PAHs were producing all the bands. However, the data could be reconciled with PAH emission if the 11.3 μm band was dominated by emission from large PAHs and the 3.3 and 3.4 μm bands were dominated by emission from small PAHs. Theoretical calculations by Schutte, Tielens, & Allamandola (1993) show this would be the case for a power law size distribution of PAH molecules.

The Orion Bar is an ideal region for studying PAH emission. Becklin et al. (1976) showed that the Bar was bright and extended at 10 μm, and described it as a nearly edge-on transition zone between an H II region created by the Trapezium stars (roughly to the north) and neutral gas (to the south). Aitken et al. (1979) showed that the 10 μm emission was dominated by the PAH emission bands. Bregman et al. (1989) showed the series of narrow bands all had similar spatial distributions which differed from the spatial distribution of the underlying broad plateaus. While the narrow bands peaked just outside the ionized region, the broad plateaus also existed well within the ionized region. This behavior suggested that the narrow bands arose from PAH molecules that had shorter lifetimes in the harsh UV field near the Orion Bar than the larger PAH clusters which produced the broader features.

In this paper we present images of the Orion Bar region of PAH emission at three different wavelengths, the 3.3 μm C-H stretch, the 11.3 μm C-H bend, and at 8.4 μm on the long

[1] Space Sciences Division, MS 254-6, NASA Ames Research Center, Moffett Field, CA 94035-1000.
[2] UCO and Lick Observatory, UCSC, Santa Cruz, CA 95064.

wavelength wing of the 7.7 μm C-C mode. The large number of data points in these images makes it possible to make a statistical comparison of the data with the Schutte et al. (1993) model for PAH emission in the Orion Bar. It is not possible to compare these data with quantitative models for QCCs or HACs, since the models don't exist for these materials. Section 2 describes the instrument and observations while § 3 discusses the model comparison and the implications for PAHs.

2. OBSERVATIONS AND INSTRUMENT DESCRIPTION

The observations were made from the NASA/University of Arizona 1.5 m telescope on Mount Lemmon in 1991 November. Two infrared cameras were used for the measurements, one with a 128 × 128 InSb array and the other with a 128 × 128 Si:Ga array. Both arrays were manufactured by Amber Engineering. The Si:Ga array requires LHe operation while the InSb detector was operated at pumped LN_2 temperatures. Anti-reflection coated lens, filter, and widow assemblies are optimized for the band pass of the two different arrays. Each camera has a filter wheel, a 38 mm f/1.5 ZnSe reimaging lens (operating at a focal reduction of 2), with field and Lyot stop baffles. The plate scales are 0.″75 pixel^{-1} for the InSb camera and 0.″96 pixel^{-1} for the Si:Ga camera. The InSb camera has six fixed filters and the Si:Ga camera has four fixed filters and a 1.8% spectral resolution 8–14 μm CVF which was used to obtain images at 8.4, 11.3, and 11.8 μm. For the 8.4, 11.3, and 11.8 μm images, the Orion Bar was chopped 90″ N-S at a frequency of 1 Hz. Frames were co-added for 60 seconds, then the telescope was nodded to allow cancellation of telescope background and offset. Using the InSb camera, images were obtained in a staring mode through bandpass filters at 3.25 ($\Delta\lambda/\lambda$ = 1.8%) and 3.3 μm ($\Delta\lambda/\lambda$ = 3.6%). The object was observed for 20 seconds, then the telescope was moved 90 arcsec south and the sky was measured. The sequence continued with the sky being sampled and then the object. An optical CCD guide camera and a gold coated dichroic beamsplitter were used, allowing for accurate guiding with a computer controlled autoguider. The autoguider reduces image motion to a fraction of an arcsecond, and ensures that the image is returned to the same place on the infrared array during nodding of the telescope.

The images at 3.3, 8.4, and 11.3 μm sample strong emission bands in the Orion Bar, while the 3.25 and 11.8 μm images sample the underlying plateaus. The 8.4 μm image is not at the peak of a PAH band (as are the 3.3 and 11.3 μm images), but rather on the long wavelength wing of the strong 7.7 μm band. We could not observe closer to the 7.7 μm peak since the shortest wavelength available on our CVF with an unvignetted field of view was 8.4 μm. The long wavelength wing of the 3.25 μm filter includes the 3.3 μm PAH emission feature. The image obtained with the 3.25 μm filter shows the same emission as the image obtained through the 3.3 μm filter, but at about 10% of the intensity, consistent with all the emission in the 3.25 μm image arising from PAH emission. The 11.8 μm image showed no emission above the noise. Thus, the images at 3.3, 8.4, and 11.3 μm show emission entirely from PAHs.

To obtain the same plate scale for all the images, the 3.3 μm image was resampled to produce an image with 0.″96 pixels. In order to create images with similar spatial resolution and to improve the signal-to-noise, each image was smoothed to the seeing limited resolution of the images by using a Gaussian filter with a FWHM of 1.5 pixels. Figure 1 (Plate 5) shows the images of the Orion Bar at 3.3, 8.4, and 11.3 μm. Camera orientation was measured by trailing a star N-S across the array while taking a long integration. The measured rotation relative to the N-S direction was 0° for the InSb camera and 3.°5 west of north (clockwise) for the Si:Ga camera. The 8.4 and 11.3 μm images in Figure 1 have been rotated 3.°5 counterclockwise. For analysis, the 8.4 and 11.3 μm frames were registered relative to the 3.3 μm frame by using the measured position of Θ^2 Ori (the bright star in the 3.3 μm image) relative to the center of the images. Errors for each image were determined by measuring the standard deviation of a few hundred sky pixels. These error bars shown in Figures 3–6 below are ±1 σ errors.

3. DISCUSSION

In order to quantitatively compare the data to published models for the Bar, we selected data points from the center of the Bar away from Θ^2 Ori, since there appears to be some PAH emission directly associated with Θ^2 Ori (most clearly evident at 11.3 μm). The selected region is contained in the box shown in Figure 2, and is 25″ along the Bar and 20″ across the Bar.

There are several striking differences between the three images. First, the Bar is wider at 11.3 μm than at 8.4 or 3.3 μm. Secondly, the brightest spots in the three images do not correspond to the same locations in the Bar. Thus, while the emission in all three bands occurs in roughly the same place (i.e., along the Bar), the details of the emission are different. The 3.3 μm emission is much less uniform than either the 8.4 or 11.3 μm emission, exhibiting many small bright knots. This behavior is consistent with emission from PAHs since the strength of the 3.3 μm band is much more sensitive to excitation of the molecules than the longer wavelength bands. Also, the 3.3 μm band is dominated by emission from the smallest PAHs which are most easily destroyed by UV photons, and thus may be most abundant in high-density knots in the Bar. The PAH emission is confined to the Bar presumably since the molecules have short lifetimes in the H II region toward the north (Bregman et al. 1989), while UV absorption by material in the Bar has depleted the supply of exciting photons toward the south.

For PAHs, the 3.3 and 11.3 μm bands should correlate, on the average, since they both come from the same C-H bonds,

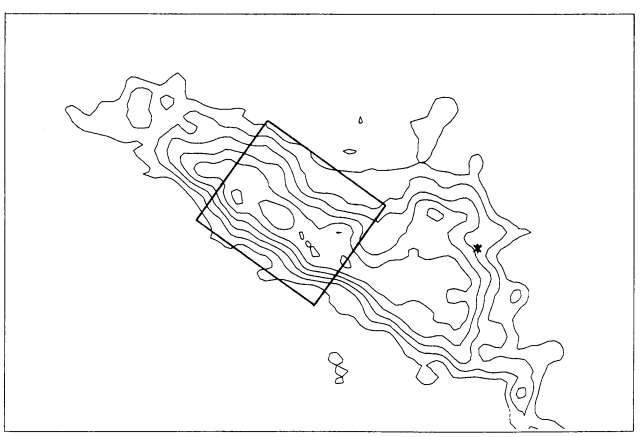

FIG. 2.—Contour map of the 11.3 μm image of the Orion Bar. The lowest contour is 90 mJy pixel^{-1} and the contour intervals are 20 mJy pixel^{-1}. The 1 σ noise level is 11 mJy/pixel^{-1}. The star indicates the position of Θ^2 Ori. The data points used for analysis are contained in the rectangle.

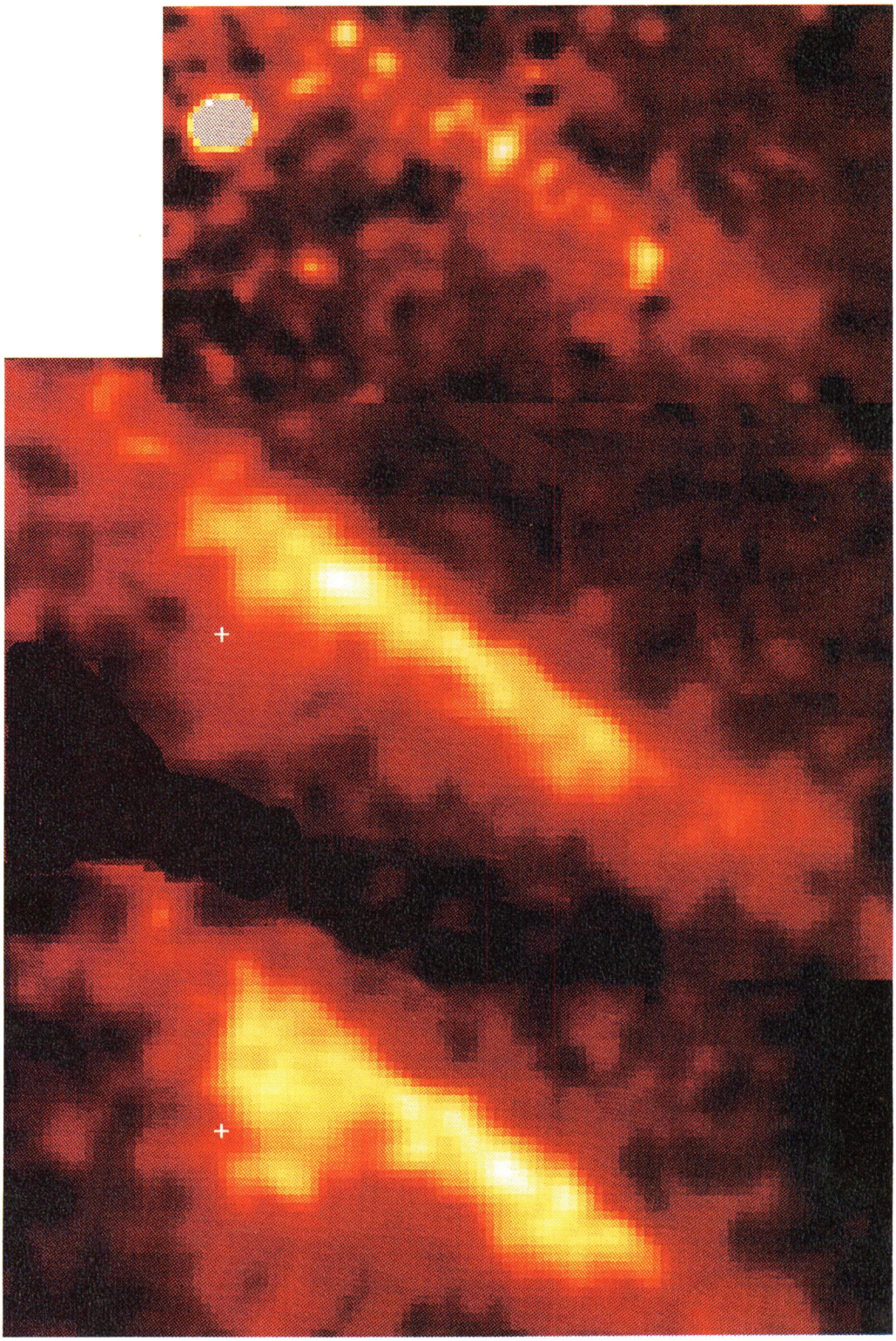

FIG. 1.—Images of the Orion Bar taken through narrow-band filters centered at 3.3, 8.4, and 11.3 μm. The brightest regions are bright yellow, while the faintest regions are dark red. Θ^2 Ori is the bright star in the 3.3 μm image, while its position in the 8.4 and 11.3 μm images is indicated by the white plus.

BREGMAN et al. (see 423, 327)

while the 8.4 and 11.3 μm bands need not correlate as well since the 8.4 μm band is a C-C mode while the 11.3 μm band is a C-H mode. However, if the mixture of PAHs does not change substantially across the bar and dehydrogenation is not severe, then the 8.4 and 11.3 μm bands should correlate quite well.

In order to examine the average spatial behavior of the three bands, averages were created for 20 rows parallel to the front of the bar for each of the three images, with each average containing 25 data points. Rows parallel to the Bar were chosen since, to first order, the UV field should be similar for all the data points within a row. Figure 3 shows the correlation of the 3.3 and 11.3 μm bands and the 8.4 and 11.3 μm bands. The pre-

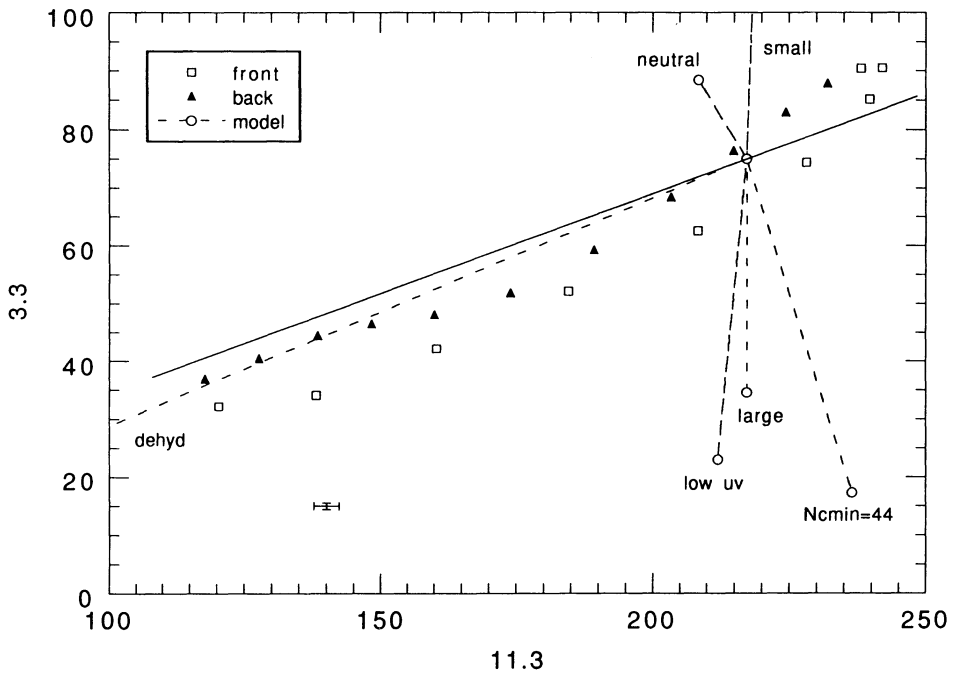

FIG. 3a

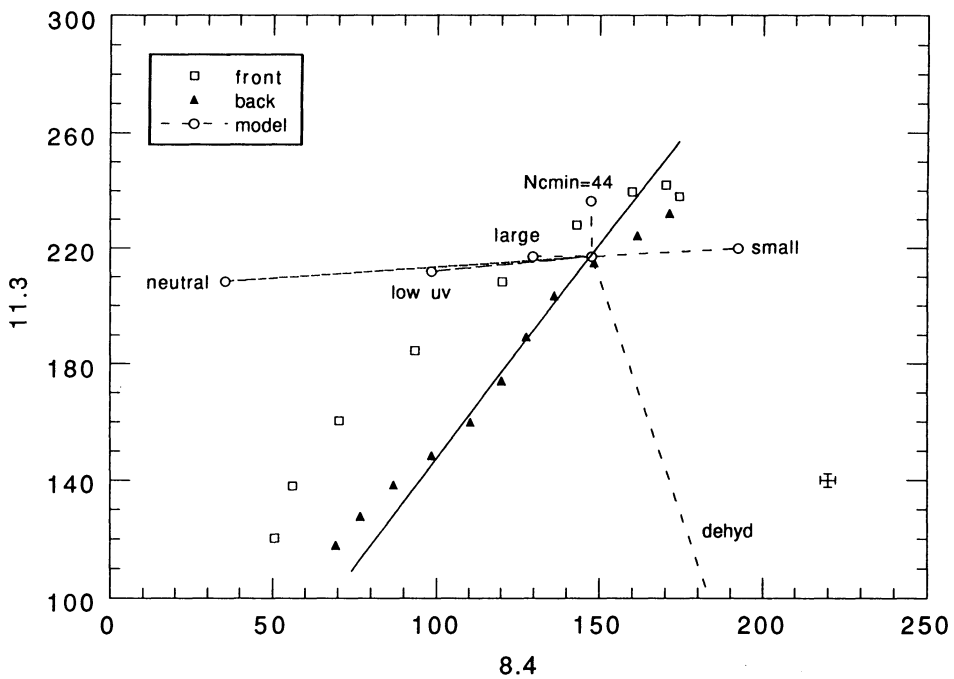

FIG. 3b

FIG. 3.—Correlation between the 3.3 and 11.3 μm bands is shown as open squares (front of Bar) and filled triangles (back of Bar) for row averages. Each data point is the average of 25 data points along a row parallel to the front of the Bar. The solid line (the trend line) indicates a 1:1 correlation in band strength. The dashed lines show the direction and magnitude of changes in the band strengths predicted by a fluorescent PAH model when various model parameters are changed. (*b*) Correlation between the 8.4 and 11.3 μm bands is shown as open squares. The other lines are the same as for Fig. 3*a*.

sumed C-H modes (3.3 and 11.3 μm) correlate with each other somewhat more tightly than the C-C and C-H modes (8.4 and 11.3 μm). Both plots show a separation between the front and back of the Bar, with the 11.3 μm band stronger on the front of the Bar relative to the 3.3 and 8.4 μm bands. This effect is more pronounced in the 11.3 vs. 8.4 μm band plot. Such tight correlations for the average band strengths are required if the emission is due to PAHs, and thus strongly supports a PAH origin for the narrow bands.

3.1. *A Quantitative Model for the Bar*

The grid of PAH emission spectra for the Orion Bar calculated by Schutte et al. (1993) can be used to investigate whether fluorescent excitation PAH models can describe the detailed behavior of the data. To make the comparison, the data were plotted along with the model calculations. In Figure 3, the solid line (which we will subsequently refer to as the trend line) indicates the trend expected if an increase in strength of one band is correlated with a similar increase in strength of the other band (i.e., if the 3.3 μm band strength doubles, then the 11.3 μm band strength should also double). Such a 1:1 correlation is expected if the band strength variations are just due to changes in the amount of material along the line of sight. The dashed lines show the model predictions for the direction and magnitude of changes in the band strengths as the model parameters are changed. These lines are vectors with their length proportional to the magnitude of the change expected by varying the indicated parameter by a fixed amount. For example, the point labeled "small" in the 3.3 versus 11.3 μm band strength plot shows the change in the 3.3 and 11.3 μm band ratio when the slope of the power law describing the PAH size distribution is changed from -3.5 to -4.5 for all the PAHs along the line of sight. If the slope is changed to -4 or if only half of the PAHs along the line of sight have the smaller size distribution, then the expected band strength changes would be smaller in magnitude, but have the same direction in the plot. The standard model was normalized to the average band strengths near the center of the Bar since Schutte et al. had fitted the model to a mid-Bar spectrum. The standard model can be normalized to any point along the solid trend line in these band-band plots.

Schutte et al. use several parameters in their model which they vary to investigate how the calculated PAH spectrum is affected by variations of the parameters. They use a power-law distribution to describe the PAH size distribution, with $n(a) \propto a^{-\alpha}$ where $n(a)$ is the number of PAHs with radius a and $\alpha = 3.5$ in the standard model. The model points labeled "small" ($\alpha = 4.5$) and "large" ($\alpha = 2.5$) indicate the trends in band strength when the slope of the power law describing the PAH size distribution is changed to increase the relative amounts of either small or large PAHs. The point labeled "low uv" has an exciting star temperature of 10,000 instead of 40,000 K. Deletion of PAHs with fewer than 44 carbon atoms is shown by the point labeled "Ncmin = 44." To fit the Bar spectrum, Schutte et al. found it necessary to increase the PAH absorption cross sections above those measured in the laboratory. They speculated that the increased cross sections might be due to ionization of the PAHs. The point labeled "neutral" shows what happens to the band strengths when the laboratory cross sections are used. Dehydrogenation of the PAHs by 95% is indicated by the point labeled "dehyd."

3.2. *Band-Band Correlations*

Perhaps the simplest way to examine the observational data is to plot band strengths against each other (i.e., band-band plots). If the PAH properties are the same at all locations in the Bar and the excitation is constant, then these plots should just be straight lines (shown as solid lines in Fig. 3) since the band strengths would only depend on the number of PAHs along the line of sight. Deviations from this trend line indicate changes in PAH properties or excitation. The sensitivity of the band strengths to the model parameters depends on which bands are plotted. In the comparison of the C-H modes in Figure 3 (3.3 and 11.3 μm images), the linear trend line is followed for the data points toward the front and back of the Bar. However, in the center of the Bar, where the bright 3.3 μm emission knots occur, the 3.3 μm band strength grows more rapidly than the 11.3 μm band strength. The model indicates that the strongest effect in this direction is produced by increasing the number of small PAHs in the center of the Bar relative to the front or back of the Bar. Plotting other band-band ratios can help to sort out which effects are most important, since the directions and magnitudes of the different vectors depends on which bands are plotted.

While row averages are useful for examining average trends, they smooth out the details and give little information about the range of band intensities present in the data. For examining the details present in the images, a data set was created by averaging pairs of data points from adjacent rows, thus reducing the number of data points displayed in the plots and increasing the signal-to-noise of each point. Spatial resolution is not degraded by this procedure since smoothing of the images combined with the 1".5 diffraction limit of the telescope at 11.3 μm reduces the spatial resolution to about 2". Figure 4*a* shows, once again, the comparison of the 3.3 and 11.3 μm bands with the Bar model. Deviations from the trend line are much larger than expected from just statistical errors (as indicated by the $\pm 1\ \sigma$ error bars). Generally, the effects of "low uv," "large," and "Ncmin = 44" all have similar effects. "low uv" would only be expected for the points toward the back of the Bar away from the Trapezium stars, while "large" and "Ncmin = 44" both have a deficiency of small PAHs. Except for dehydrogenation, which moves the points along the trend line and therefore cannot be separated from the first-order effect of varying amounts of material along the line of sight, all the other effects of changing the parameters tend to move the data points more or less in a direction perpendicular to the trend line. The PAH size distribution is the most important effect, and probably accounts for the spread of data points. The points spread nearly evenly above and below the trend line except for the points near the center of the Bar (rows 4 and 5) which appear to have an excess of small PAHs relative to the other Bar regions.

Figure 4*b* shows the comparison of the 11.3 and 8.4 μm images. The direction and magnitude of the changes in the expected band intensities resulting from varying the parameters is quite different than for the 3.3 versus 11.3 μm images. Significant dehydrogenation should have a large effect, but none is observed. Changing the cross sections from those used to "neutral" has a large effect, and may account for the location of the points at the front of the Bar (row 2) to the left of the trend line. PDR models (Bakes & Tielens 1994) indicate that the charge of PAHs would be zero (neutral) along the front of the Bar, but have a negative charge within the Bar. The data points toward the back of the Bar (rows 9 and 10) are also to

the left of the trend line, but not as far to the left as are the points along the front of the Bar. These are the points for which the UV field is the weakest, and the model indicates that a weaker (and cooler) UV field should result in data points to the left of the trend line. While it is possible from this figure to conclude that these points have neutral cross sections similar to the points along the front of the Bar, Figure 6*a* shows that these same data points are only consistent with either a larger PAH population than average or "low uv." The points along the back of the Bar are probably showing the effects of absorption of UV photons through the Bar rather than the effects of having a larger PAH population than average.

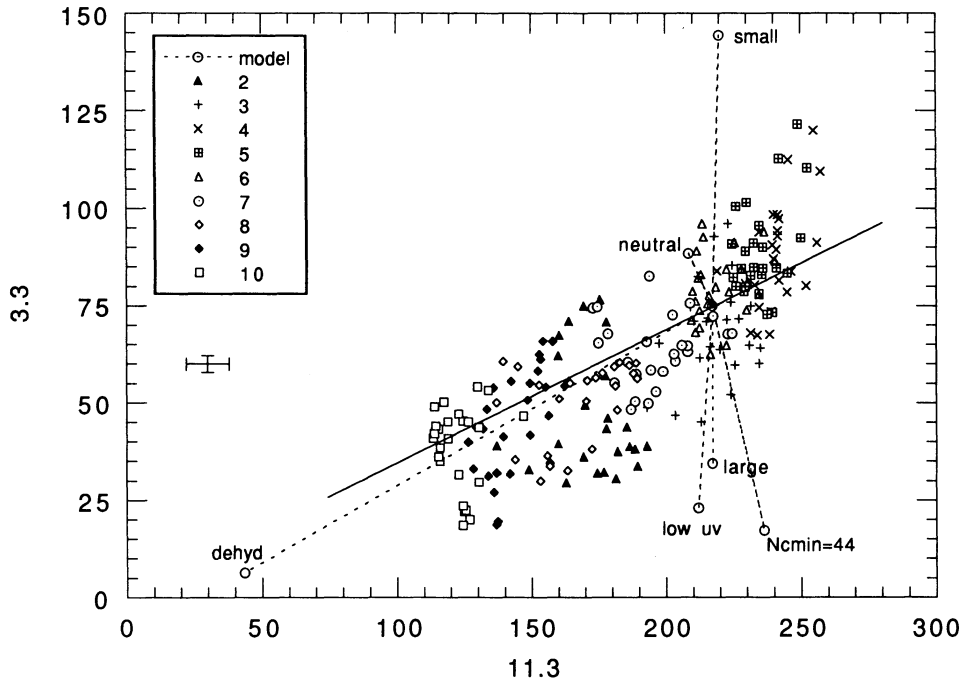

FIG. 4*a*

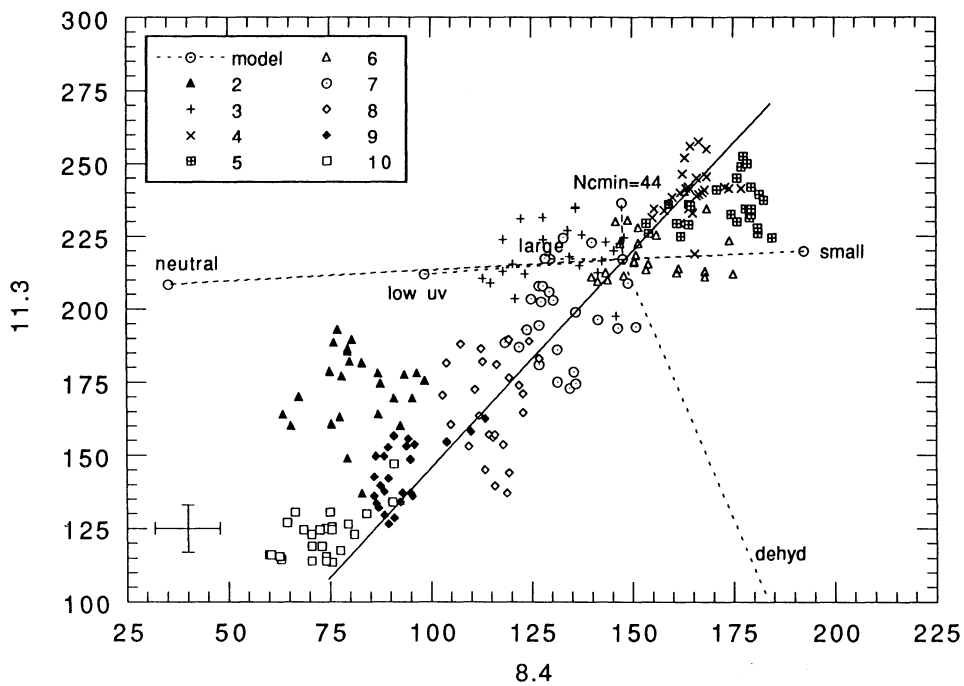

FIG. 4*b*

FIG. 4.—Correlation between the 3.3 and 11.3 μm bands for individual data points. The different symbols for the data points correspond to increasing distance into the Bar, so the points labeled "2" in the legend are near the front of the Bar while the points labeled "10" are toward the back of the Bar away from the Trapezium stars. (*b*) Correlation between the 8.4 and 11.3 μm images for individual data points, similar to Fig. 4*a*.

3.3. *Band-Band Ratios*

Ratios of two images can be used to remove the first order effect of differing amounts of material along the line of sight. Figures 5 and 6 show these band ratio plots. In Figure 5*a*, the ratio of the 3.3/8.4 μm images is plotted against the ratio of the 3.3/11.3 μm images using the row averaged data. The statistical errors are shown as ± 1 standard deviation, and for Figure 5*a* are about equal to the size of the data points. About half of the data points spread out in the direction expected for a varying size distribution of PAHs. The other half of the points are located to the upper left of the standard model, with the most deviant points being those along the front of the Bar. The model indicates that points can occupy this part of the plot

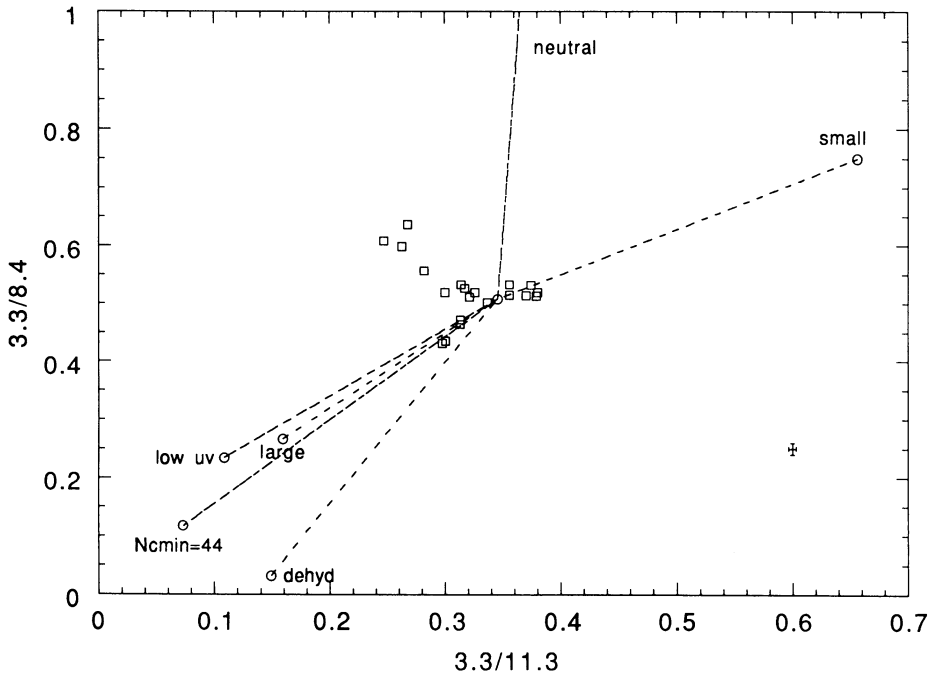

FIG. 5*a*

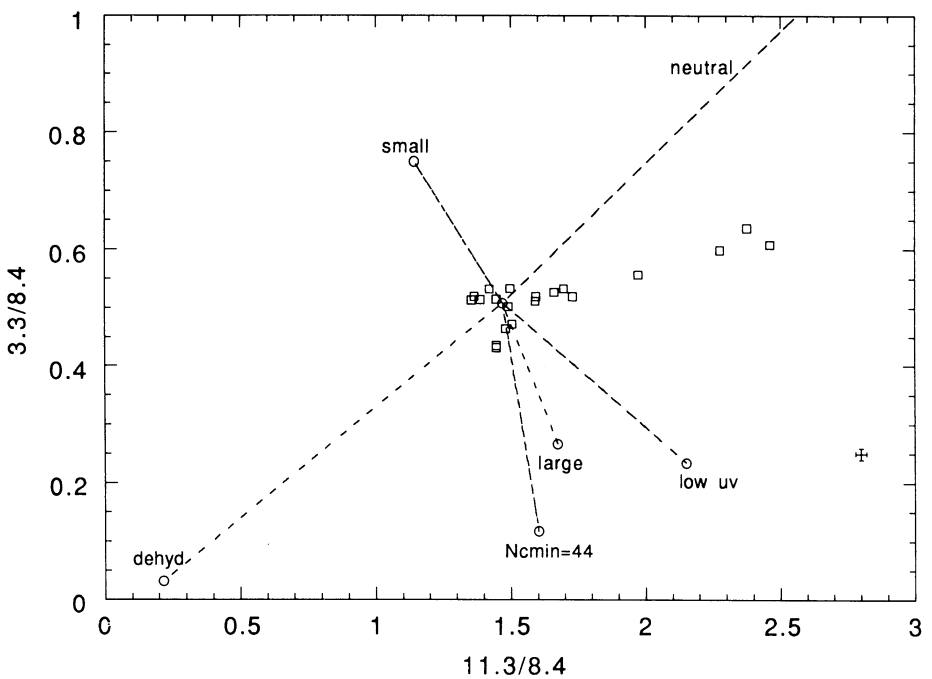

FIG. 5*b*

FIG. 5.—(*a*) Band-band ratio correlations between the 3.3/8.4 μm and 3.3/11.3 μm ratio images using row-averaged data. (*b*) Band-band ratio correlations between the 3.3/8.4 μm and 11.3/8.4 μm ratio images using row-averaged data.

only by having neutral cross sections in combination with one or more of the four variables which would move the data points to the lower left (low uv, large, Ncmin = 44, dehydrogenation). However, "low uv" is not expected for the points along the front of the Bar. In Figure 5*b*, most of the data points are clustered near the standard model point, while the data for the front of the Bar are to the right. A combination of neutral cross sections plus more large PAHs (i.e., large or Ncmin = 44) could account for the observed data, but dehydrogenation is ruled out since it would move the points in a direction opposite to the observed trend.

Figures 6*a* and 6*b* show the same band-band ratio plots for the unaveraged data. Most of the data points lie along the line expected just from a changing size distribution of PAHs. The

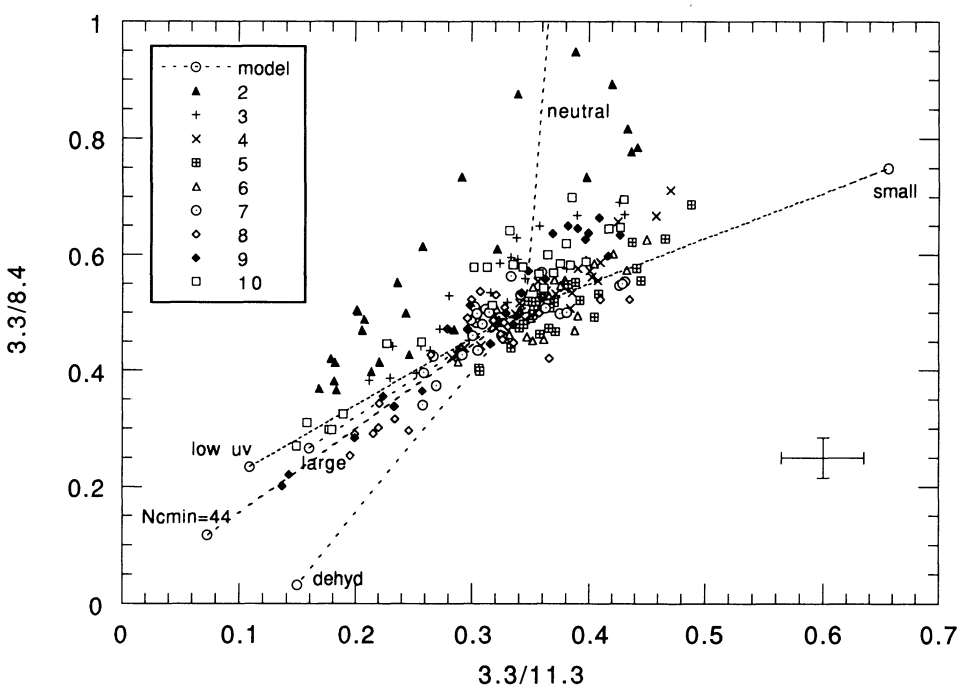

FIG. 6*a*

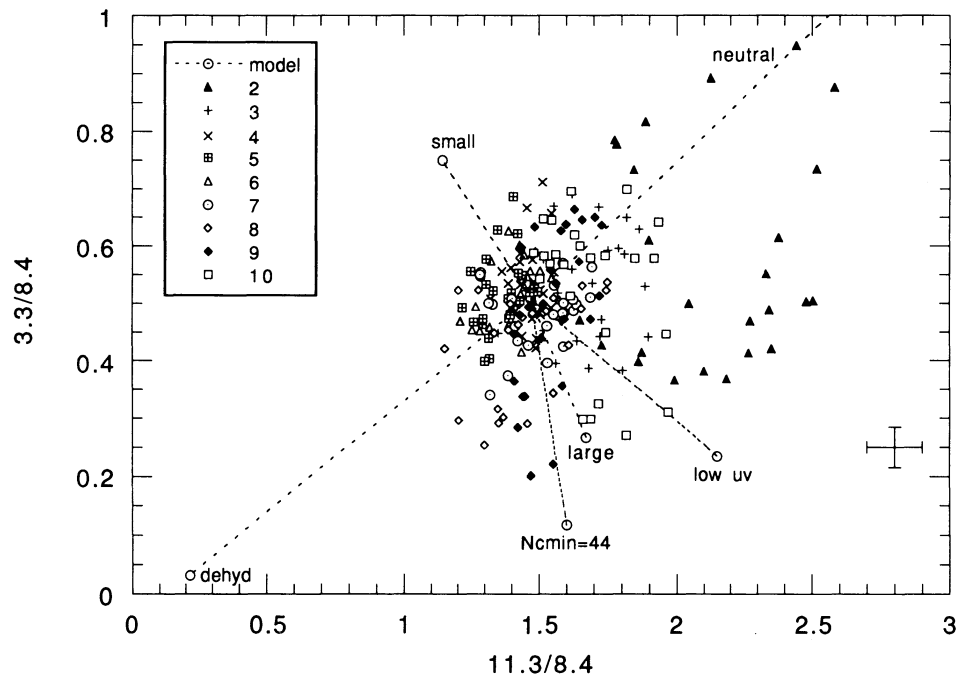

FIG. 6*b*

FIG. 6.—(*a*) Same as Fig. 5*a* except the individual data points are shown, not averaged data. (*b*) Same as Fig. 5*b* except the individual data points are shown, not averaged data.

front Bar points (row 2) lie substantially above the other data points, once again in the direction expected for "neutral" emission cross sections. While the average for the points along the front of the Bar indicates a PAH size distribution with more large PAHs than average, Figure 6*a* shows that these points have a range of PAH size distributions similar to the rest of the Bar. Data points toward the back of the Bar show a large range in band-band ratios in the direction expected for "low uv" or large PAHs. These are the points which would be expected to be most affected by absorption of UV photons within the Bar. Figure 6*b* results in a similar conclusion for the points along the front and back of the Bar.

4. CONCLUSIONS

We have obtained images of the Orion Bar through narrow band filters set at 3.3, 8.4, and 11.3 μm. The 3.3 and 11.3 μm images show emission from the C-H stretching and bending modes of PAHs while the 8.4 μm image samples the long wavelength wing of the 7.7 μm band from C-C vibrations. The 3.3 μm image shows small bright knots of emission unlike the more uniform emission observed at 8.4 and 11.3 μm. The 11.3 μm image shows a Bar which is somewhat broader than at the other wavelengths.

In order to analyze the data and allow a comparison with a model, a data set was created from a section of the Bar comprised of intensities for 250 locations at each of the three wavelengths. To first order, the intensities of the three bands correlate very well as is required if the emission is from PAHs. The data set was also compared with the model calculated by Schutte et al. (1993) for fluorescent PAH emission from the Orion Bar. From this comparison we conclude that:

1. The size distribution of PAHs varies within the Bar.
2. The points along the front of the Bar have emission cross sections characteristic of neutral PAHs, while within the Bar the emission cross sections are different, indicating charged PAHs.
3. The PAHs along the front of the Bar are larger than average for the Bar.
4. The PAHs which produce the bright emission knots at 3.3 μm are smaller than average.
5. Emission along the back of the Bar is consistent with PAH emission in a region with a cooler UV spectrum than in the Bar center and/or a population of larger PAHs than average.
6. There is no evidence for dehydrogenation of PAHs.

We wish to thank Scott Sandford, Doug Hudgins and Laura Kay for their help with the camera observations. We are also indebted to the Mt. Lemmon staff for helping to prepare the telescope for operation.

REFERENCES

Aitken, D. K., Roche, P. F., Spencer, P. M., & Jones, B. 1979, A&A, 76, 60
Allamandola, L. J., Bregman, J. D., Sandford, S. A., Tielens, A. G. G. M., Witteborn, F. C., Wooden, D. H., & Rank, D. 1989, ApJ, 345, L59
Allamandola, L. J., Tielens, A. G. G. M., & Barker, J. R. 1985, ApJ, 290, L25
Bakes, E. L. O., & Tielens, A. G. G. M. 1994, in preparation
Becklin, E. E., Beckwith, S., Gatley, I., Matthews, K., Neugebauer, G., Sarazin, C., & Werner, M. W. 1976, ApJ, 207, 770
Bregman, J. D. 1989, in IAU Symp. 135, Interstellar Dust, ed. L. J. Allamandola & A. G. G. M. Tielens (Dordrecht: Kluwer), 109
Bregman, J. D., Allamandola, L. J., Tielens, A. G. G. M., Geballe, T. R., & Witteborn, F. C. 1989, ApJ, 344, 791
Bregman, J. D., Rank, D., Temi, P., Hudgins, D., & Kay, L. 1993, ApJ, 411, 794
Cohen, M., Allamandola, L., Tielens, A. G. G. M., Bregman, J., Simpson, J., Witteborn, F. C., Wooden, D., & Rank, D. 1986, ApJ, 302, 737
Duley, W. W., & Williams, D. A. 1981, MNRAS, 196, 269
Leger, A., & Puget, J. L. 1984, A&A, 137, L5
Robertson, J., & O'Reilly, E. P. 1987, Phys. Rev. B., 35, 2946
Roche, P. F., Aitken, D. K., & Smith, C. H. 1989, MNRAS, 236, 485
Sakata, A., Wada, S., Tanabe, T., & Onaka, T. 1984, ApJ, 287, L51
Schutte, W. A., Tielens, A. G. G. M., & Allamandola, L. J. 1993, ApJ, 415, 397
Witteborn, F. C., Sandford, S. A., Bregman, J. D., Allamandola, L. J., Cohen, M., Wooden, D. H., & Graps, A. L. 1989, ApJ, 341, 270